Chapter 9
MEMS Nanopositioners

Jason J. Gorman

9.1 Introduction

Nanopositioning mechanisms, or nanopositioners, have evolved quickly over the last few decades due to a growing need for nanoscale precision motion control in applications including microscopy, lithography, nanomanufacturing, and optics. The critical differentiator between nanopositioners and other motion stages is that nanopositioners are capable of nanoscale positioning resolution, which is generally interpreted as a few nanometers and below. Motion stages with mechanical elements that have friction, such as screws, linear bearing slides, and rotational bearings, are not capable of nanoscale resolution. The backlash caused by friction limits the precision in these mechanisms to tens of nanometers, and complex control systems are often required to reach this level. As a result, nanopositioner designs typically use a flexure mechanism to guide the motion of the stage, which exhibit no friction since the motion is based on structural bending, thereby providing continuous smooth movements.

The simplest nanopositioner is composed of a flexure mechanism and an actuator that drives the mechanism. In most high-precision applications, nanopositioners also include sensors for measuring the motion, which are used for feedback control and other error compensation methods. Among the many nanopositioner designs in the literature, the combination of piezoelectric actuators, a metal flexure mechanism, and capacitive or optical sensors is by far the most common. This combination can be seen in numerous linear, multi-axis, and rotational nanopositioners [1–3] and has been the basis of the majority of commercially available nanopositioners [4–6].

J.J. Gorman (✉)
National Institute of Standards and Technology, 100 Bureau Drive,
Stop 8212, Gaithersburg, MD 20899-8212, USA
e-mail: gorman@nist.gov

C. Ru et al. (eds.), *Nanopositioning Technologies*,
DOI 10.1007/978-3-319-23853-1_9

These motion stages have radically improved the performance of many precision instruments, including scanning probe microscopes [7] and optically lithography tools for semiconductor electronics manufacturing [8].

In tandem with the evolution of nanopositioners over the last few decades, microelectromechanical systems (MEMS) have emerged to create a major industry and have enabled numerous technology advances including automotive airbag deployment, inertial navigation for unmanned vehicles, and smartphones. Most MEMS are composed of combinations of actuators, flexure mechanisms, and sensors, as seen in accelerometers, gyroscopes, and resonators. Furthermore, these devices have been shown to be capable of exceptional precision compared to their macroscale counterparts. As a result, MEMS are an obvious technology platform for extending the capabilities of nanopositioners. This opportunity was realized early on in the development of both nanopositioners and MEMS by Akamine et al. [9] who developed a microscale piezoelectric cantilever for scanning tunneling microscopy that can move with three degrees of freedom. Since then, MEMS nanopositioners have progressed rapidly due to exciting applications that are not possible with macroscale nanopositioners, including multi-tip scanning probe microscopy (SPM) for high-bandwidth imaging, lithography, and data storage.

This chapter will provide a review of the state of the art for MEMS nanopositioners. The next section discusses the motivation for using MEMS in nanopositioning, including the components within a nanopositioner, the performance requirements for these systems, the advantages in using MEMS to create high-performance motion stages, and the applications that are driving the development of this technology. This is followed by a review of the actuators and sensors that have been demonstrated in MEMS nanopositioners, with an emphasis on the advantages and disadvantages related to precision motion control. An assessment of the performance of MEMS nanopositioners to date in terms of resolution, range, bandwidth, and size is then presented. Finally, the chapter concludes with thoughts on the current limitations and future directions for MEMS nanopositioners.

9.2 Motivation for MEMS Nanopositioners

Nanopositioners are composed of actuators, a flexure mechanism, sensors, and a control system. The block diagram in Fig. 9.1 describes the interactions between these components. For a single-axis system, a control voltage, u, is amplified and applied to the actuator. This causes the actuator to exert a force, F, on the flexure mechanism, thereby causing a displacement, x. The displacement is then measured with the sensor and the sensing signal is processed by the readout electronics to produce a voltage, V_x, which is proportional to the displacement. The sensor voltage is then sent to the control system, which generates the control voltage, u, based on the selected algorithm. Open-loop control is also possible but it typically yields significantly reduced precision.

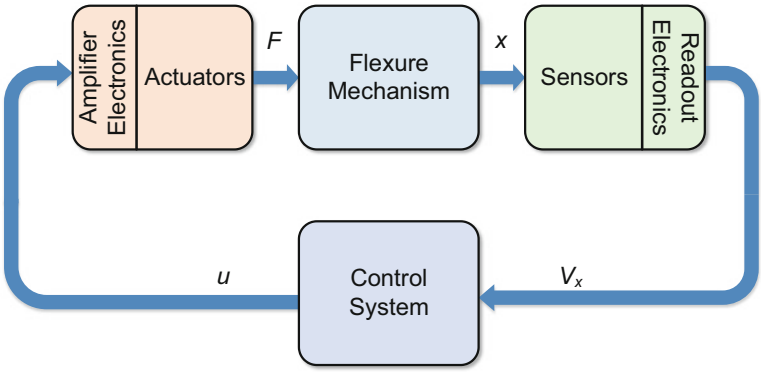

Fig. 9.1 Anatomy of a nanopositioner. Block diagram showing the components within a nanopositioner and the interactions between the components. u = control voltages, F = forces applied by actuators, x = displacements of MEMS nanopositioner, V_x = measured displacements in voltage

Actuators for controlled motion and sensors for displacement measurement are widely used in MEMS including those found in accelerometers, gyroscopes, microphones, and pressure sensors. As a result, MEMS technologies provide a compelling approach to implementing the device anatomy shown in Fig. 9.1. The main question is whether MEMS nanopositioners can match the performance obtained by macroscale nanopositioners. While there is considerable variation in the performance attained with macroscale nanopositioners, the motion resolution can be as good as 0.05 nm, the range can be as high as a few hundred micrometers, and the dynamic range is typically above 10^5. The achievable motion bandwidth ranges from tens of hertz to several kilohertz and is inversely related to the motion range. There are hard constraints between these four metrics (resolution, range, dynamic range, and bandwidth) but they can be optimized for a given application. For example, scanning tunneling microscopy (STM) usually requires greater resolution than atomic force microscopy (AFM). Therefore, a nanopositioner for STM may have motion resolution on the order of tens of picometers but with a range of only a few micrometers, whereas a nanopositioner for AFM may have sub-nanometer resolution and a range around 100 μm.

The motivation for the development of MEMS nanopositioners is a combination of advantages related to performance, functionality, and new applications that are only accessible with small mechanisms. Scaling down in size presents one set of advantages. First, MEMS have high resonant frequencies compared to larger systems, resulting in greater motion bandwidth. Second, MEMS can be integrated on a silicon chip with other technologies, such as electronics and photonics, thereby providing a path to low-power embedded systems with high functionality. Finally, arrays of nanopositioners can be fabricated on a single chip and controlled independently. The main disadvantages in scaling down in size are the resulting payload size and mass limits.

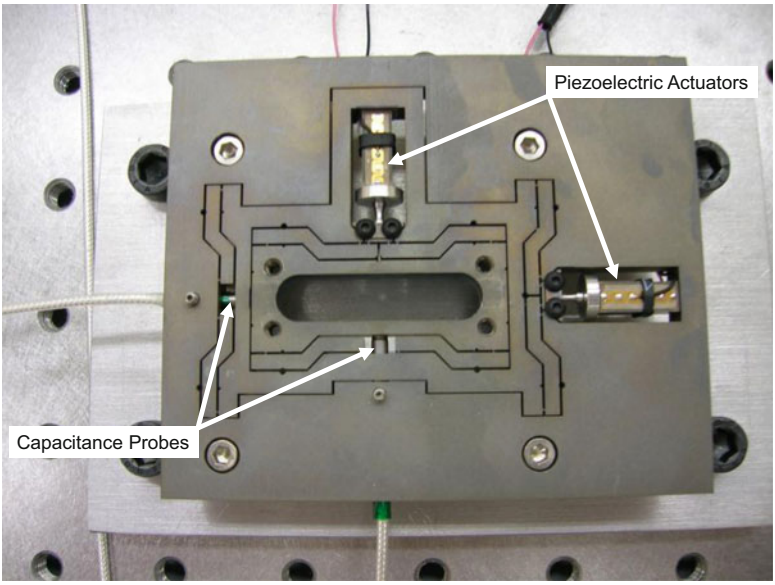

Fig. 9.2 An *XY* nanopositioner with piezoelectric actuators, a nested flexure mechanism with motion amplification, and capacitance probes (J.J. Gorman, S. Bergna, N.G. Dagalakis, unpublished)

Another set of advantages results from the integration and economy of scale inherent in MEMS fabrication processes. A representative macroscale *XY* nanopositioner is shown in Fig. 9.2. It includes two piezoelectric stack actuators, a nested *XY* flexure mechanism that amplifies the actuator motion, and two capacitive position sensors. The flexure mechanism is fabricated using wire electrodischarge machining (wire EDM), which is a slow, expensive, and serial process. The actuators and sensors are assembled into the mechanism by hand, adding additional time and cost to fabrication. Additionally, misalignment between components is inevitable, causing off-axis forces and erroneous position measurements, thereby reducing the accuracy of motion. In comparison, MEMS fabrication uses parallel processes, the mechanisms are typically monolithic, and assembly is not required. Therefore, the cost is significantly reduced and motion errors due to misalignment of sensors and actuators are all but eliminated.

Figure 9.3 shows an *XY* MEMS nanopositioner with electrothermal actuators and a nested flexure mechanism that amplifies motion, similar to the mechanism shown in Fig. 9.2. Comparing Figs. 9.2 and 9.3, the advantages of MEMS fabrication are evident. The MEMS nanopositioner is fabricated in a single layer of single-crystal silicon. Complex flexure mechanisms, such as the multi-lever arm design with circular notch flexure joints can be fabricated with ease using deep reactive ion etching (DRIE). The actuators and flexure mechanism are directly integrated and the only misalignments possible between the two are caused by lithography errors,

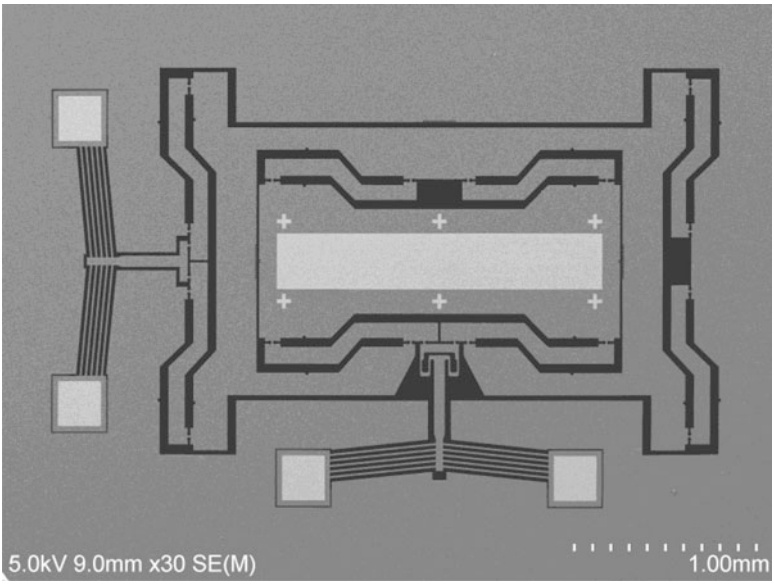

Fig. 9.3 An *XY* MEMS nanopositioner with electrothermal actuators and a nested flexure mechanism with motion amplification, similar to that shown in Fig. 9.2 (J.J. Gorman, S. Bergna, N.G. Dagalakis, unpublished)

which are typically negligible. This is in stark contrast to the complex couplings necessary to assemble the actuators and sensors in the macroscale nanopositioner in Fig. 9.2.

The materials available in MEMS fabrication also provide significant advantages over those common in macroscale nanopositioners. Single-crystal silicon is the most widely used material for MEMS nanopositioners due to several factors. It is broadly available with widely varying specifications, its material properties are well known, and there are many well-established etch processes available, making it a relatively easy material to use in MEMS fabrication. Silicon has a much higher Young's modulus and a lower coefficient of thermal expansion than the materials used in macroscale nanopositioners (i.e., metals), resulting in stiffer structures and improved thermal stable. Monolithic integration in silicon further improves thermal stability by avoiding mismatched material properties as found in assembled nanopositioners.

There are several applications driving the development of MEMS nanopositioners with SPM being the most prominent and well explored. By definition, SPM [10], including STM and AFM, requires a nanopositioner to scan the probe or sample with exceptional precision. There is a continual push to increase the scan rate in SPM in order to reduce drift in surface images, maximize data collection, and observe dynamic nanoscale phenomena. As described above, MEMS are capable of high motion bandwidth making them an obvious solution to the SPM scanning problem. Akamine et al. [9] were the first to demonstrate a MEMS multi-axis

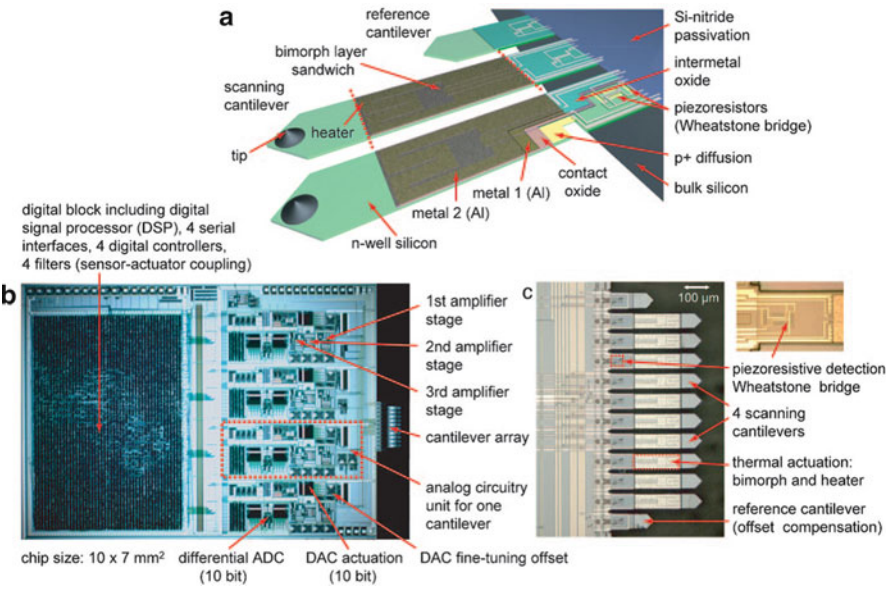

Fig. 9.4 Active AFM cantilever array. (**a**) Schematic of cantilever array showing actuation and sensing elements, (**b**) embedded readout electronics, and (**c**) fabricated cantilever array (S. Hafizovic et al. © PNAS [18])

scanner for STM, achieving atomic resolution with a piezoelectric cantilever. This work was followed by the development of multi-axis electrostatic nanopositioners with integrated tunneling tips that were designed for multi-tip STM measurements [11–13].

Most of the research on MEMS scanners has focused on AFM due to the broader applications compared to STM and the simpler imaging mechanism (i.e., tip force vs. tunneling current). Due to their small size and high level of device integration, MEMS have provided a path for active AFM cantilever arrays with independent force sensing and *Z* axis actuation [14–18] (see Fig. 9.4). In addition to the increased motion bandwidth due to scaling down in size, cantilever arrays provide multiplexed measurements that increase the image size and speed of image collection by increasing the number of cantilevers. While multiple tips can be controlled in the vertical direction (e.g., 10 cantilevers [14]), scanning of the cantilever array along the *X* and *Y* axes is performed with a macroscale nanopositioner. Arrays of independent AFM scanners (*XYZ*) would be capable of significantly higher throughput due to their higher motion bandwidth. As a step in this direction, an *XY* MEMS nanopositioner has been used to image metal patterns on the scanner with resolution and bandwidth that is competitive with traditional AFM [19–22]. Most recently, a fully integrated on-chip AFM with three axes of motion and embedded force sensing has been shown to be capable of imaging nanoscale step heights with

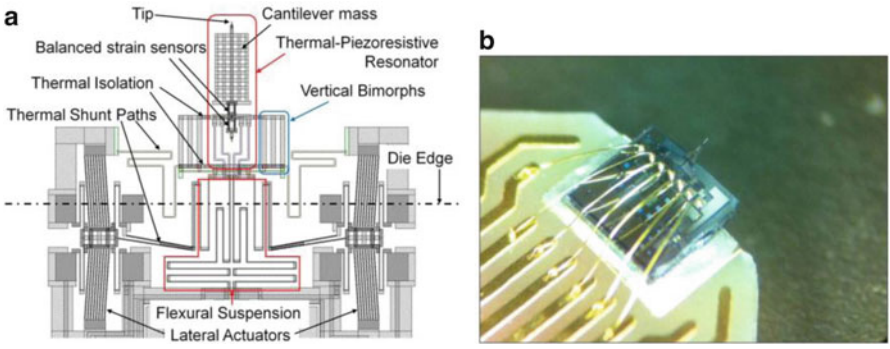

Fig. 9.5 On-chip AFM. (**a**) Schematic showing three motion axes with electrothermal actuation and cantilever with piezoresistive strain sensing and embedded tip, (**b**) fabricated on-chip AFM (N. Sarkar et al. © IEEE [24])

3 nm pk-pk vertical resolution [23, 24] (see on-chip AFM in Fig. 9.5). Applications for on-chip AFM beyond nanoscale imaging include probe-based data storage [25] and nanolithography [14].

Another active application area for MEMS nanopositioners is the manipulation of nanostructures for nanomanufacturing and material testing. A number of nanomanipulator concepts have been explored in which probes with nanoscale sharpness are used to push and tweeze nanostructures [26–29]. Nanopositioners have also been used to measure the mechanical properties of nanowires and carbon nanotubes by attaching them to the motion stage and pulling on them while observing the event in a scanning electron microscope (SEM) or transmission electron microscope (TEM) [30–32]. By scaling down the material testing experiment, the accuracy of the results can be improved due to a significant reduction in the distance between sensors and actuators and because they can more readily fit in small sample chambers as found in TEMs. Many other applications for MEMS nanopositioners are expected in the areas of adaptive optics (e.g., tunable lens arrays), photonics (e.g., laser cavity stabilization), and physics research (e.g., optical and atomic traps), among others.

Returning to Fig. 9.1, it is clear that for MEMS nanopositioners to be successful in the applications above, each of the components (actuators, flexure mechanism, sensors, controller) must perform at a level comparable to their macroscale counterparts. There has been considerable research on actuators and sensors for MEMS nanopositioners, which will be discussed in the following sections. Control system design for MEMS nanopositioners varies greatly depending on the actuator, flexure mechanism, and sensor selections, and the application of interest. As a result, this subject is discussed in detail in the following chapter. The final component in a MEMS nanopositioner, the flexure mechanism, is critical to its performance and requires careful design to achieve stable motion over the desired range. However, flexure mechanism design at the microscale is largely the same as at the macroscale (e.g., see [33, 34]), so this topic is not covered here. However, it is worth noting the variety of mechanism designs that have been used to date.

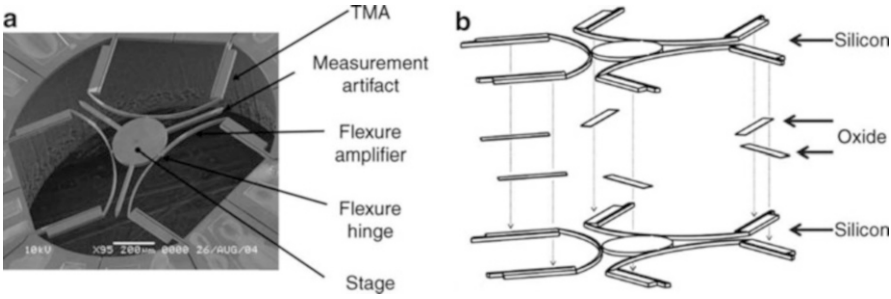

Fig. 9.6 The μHexFlex nanopositioner. This mechanism uses electrothermal actuators and a two-level flexure mechanism to generate six-axis motion. (**a**) Fabricated mechanism, (**b**) exploded diagram showing two levels of thermal actuators. (S.-C. Chen and M.L. Culpepper © Elsevier [47])

Early mechanisms relied heavily on cantilevered beams [9, 14–18] and clamped beams [35]. Double parallelogram flexures were then found to constrain the motion better than simple beam structures, resulting in pure translational motion along the degree of freedom of interest with minimal off-axis motion [35–38]. Multi-axis MEMS nanopositioners require more complex mechanisms to properly constrain the motion. A number of different designs have been used for *XY* stages, including beam structures [12, 19, 39, 40], a four-bar flexure [41], and nested structures with circular notch flexure hinges [28, 42] (see Fig. 9.3). Other multi-axis mechanisms of interest include *XYZ* stages [43–45] (see Fig. 9.8), an $XY\theta$ stage [46], and even a six-axis parallel mechanism [47], as shown in Fig. 9.6. Almost all of these flexure mechanism designs work equally well at the microscale as at the macroscale. One of the biggest challenges in developing an adequate flexure mechanism for MEMS is finding a design that is compatible with the fabrication process. In many cases, this limits the mechanism to two-dimensional geometry in the plane of the substrate, which can make it difficult to properly constrain both in-plane and out-of-plane motions simultaneously. Other important design challenges include the trade-off between range and bandwidth (i.e., fundamental resonant frequency), cross-talk between motion axes, and achieving linearity over the entire workspace.

9.3 Actuation

Actuators for nanopositioning must meet several stringent performance requirements. Smooth continuous motion with position fluctuations on the order of 1 nm or below is required. Sufficient force must be generated to move the flexure mechanism over a range from 1 to 100 μm, depending on the application. In general, a motion bandwidth of at least several hundred hertz is necessary but significantly higher bandwidth is typically expected since this is a driving motivation for using MEMS nanopositioners. Depending on the level of integration required for the application, this must all be done within a volume from 0.1 to around 5 mm^3. Actuation in

the plane of the supporting substrate and out of the plane are both required for many applications of MEMS nanopositioners, such as SPM, since they depend on multi-axis motion. There are numerous books [48, 49] and review articles [50–52] that describe the design and modeling of MEMS actuators and sensors in detail. Therefore, the goal of this section and the following section on sensors is not to provide an in-depth description on how various actuators and sensors operate. Rather, the focus is on highlighting the approaches that have been used in MEMS nanopositioners and discussing their advantages and disadvantages within this context. Among the many intriguing approaches for actuation in MEMS, almost all of the MEMS nanopositioners to date rely on electrostatic, electrothermal, or piezoelectric actuation, which are discussed below. The most obvious omission from this discussion is electromagnetic actuation, which can be very effective at the macroscale, particularly linear Lorentz force actuators. However, due to poor scaling and difficulties in fabricating microscale rare-earth magnets, electromagnetic actuation has received little attention with respect to MEMS nanopositioners, with a few exceptions (e.g., see [53] and its reference list).

9.3.1 Electrostatic Actuators

Electrostatic actuation is the most common approach for MEMS nanopositioners, as well as for MEMS in general. The design and modeling of electrostatic actuators are well understood, making them easy to integrate into mechanisms and achieve a predictable level of performance. An electrostatic actuator is a capacitor in which one side of the capacitor can move because it is attached to a flexure mechanism. When a voltage is applied across the capacitor a charge is generated, resulting in an electrostatic force that is proportional to the voltage squared. The three most common types of electrostatic actuators are the comb actuator, the parallel-plate actuator, and the parallel-plate actuator with comb structure, as shown in Fig. 9.7.

The electrostatic comb actuator (Fig. 9.7a) uses a pair of interdigitated combs to generate a force in the direction parallel to the comb fingers (i.e., the x-axis). Numerous MEMS nanopositioners have used this actuator due to its simplicity of design, well-characterized force model, and considerable motion range [12, 19, 35–41, 43, 44, 46]. An example of an *XYZ* MEMS nanopositioner with comb actuators for the X and Y axes is shown in Fig. 9.8. The force can be optimized by minimizing the gap between the fingers, g, and maximizing the thickness thickness, t. Fabrication on silicon-on-insulator wafers using DRIE is the best method for achieving these high aspect ratio structures. Although the force is proportional to the voltage squared, the actuator response can easily be linearized by canceling the nonlinearity with a square root function, either with an analog circuit or digital signal processor. The motion range of a comb actuator can be several hundred micrometers through careful design of the connected flexure mechanism [54, 55], which is exceptionally large for MEMS nanopositioners. Most comb actuators are designed for in-plane motion, but out-of-plane motion (z axis) can also

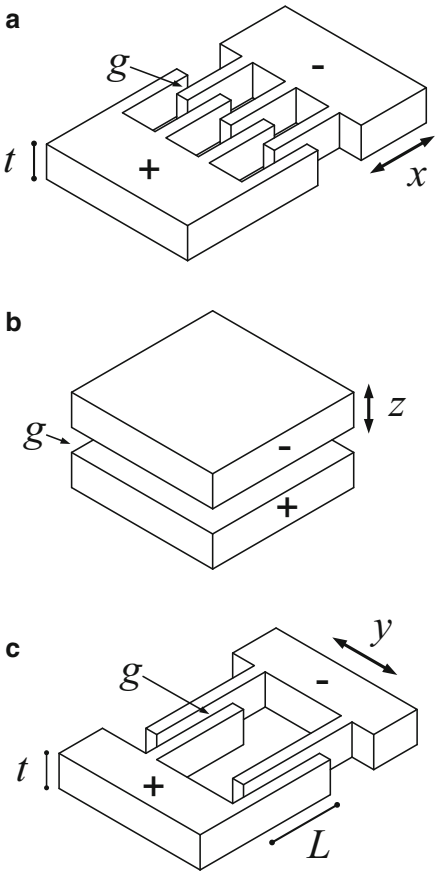

Fig. 9.7 Common electrostatic actuator designs: (**a**) Comb actuator, (**b**) parallel-plate actuator, and (**c**) parallel-plate actuator with a comb structure

be achieved by using the levitation effect [13] or an offset in the vertical position of the two combs [56, 57]. This results in a much smaller motion range, typically on the order of a few micrometers.

The electrostatic parallel-plate actuator (Fig. 9.7b) has been used at many scales and its application in MEMS predates the use of comb actuators. Several actuator geometries for in-plane [11] and out-of-plane motion [43, 58–61] have been used in MEMS nanopositioners. An example is shown in Fig. 9.8, where the parallel-plate actuator drives the Z axis of an XYZ MEMS nanopositioner. The design of this actuator is simple and easy to fabricate. However, the force generated by a parallel-plate actuator is nonlinearly related to the displacement of the moving plate, resulting in a pull-in instability, which is generally not an issue for comb actuators. The instability causes the moving plate to snap in to the stationary plate when the displacement due to an applied voltage exceeds one third of the nominal gap, g. The motion range before pull-in can be improved through mechanical design (e.g., see [62]), but it is still small compared to comb actuators. When g is made larger to accommodate a greater range, the required input voltage necessary to achieve a long

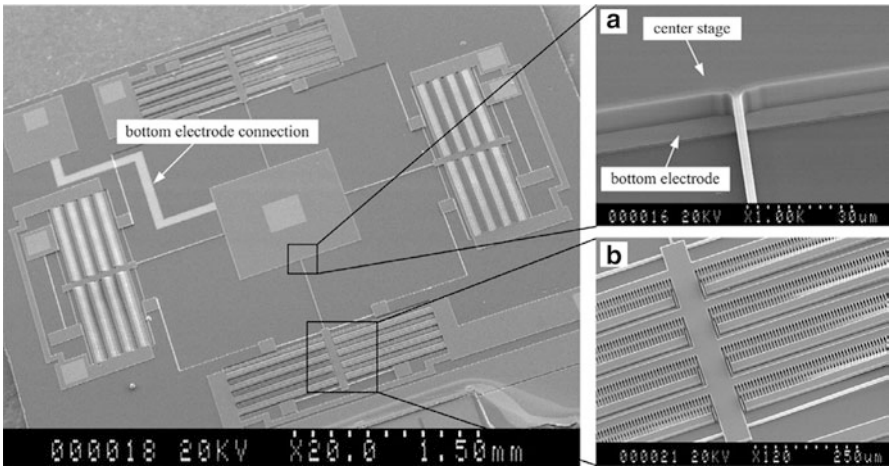

Fig. 9.8 An *XYZ* MEMS nanopositioner that uses electrostatic comb actuators for the *X* and *Y* axes and an electrostatic parallel-plate actuator for the *Z* axis (X. Liu, K. Kim, and Y Sun © IOP [43])

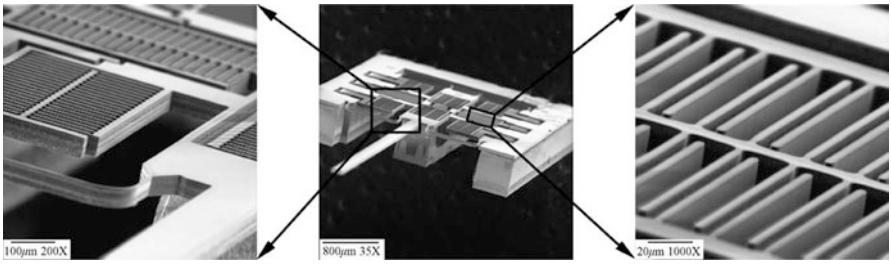

Fig. 9.9 An *XY* MEMS nanopositioner that uses electrostatic parallel-plate actuators with a comb structure (Y. Sun et al. © Elsevier [64])

range increases and becomes impractical, thereby setting the motion limit to only a few micrometers. The parallel-plate approach is typically used for out-of-plane actuation but it can be implemented for in-plane motion by using a comb structure with many parallel-plate actuators working in parallel, as shown in Figs. 9.7c and 9.9 [63, 64].

Among the many positive attributes for electrostatic actuation, possibly the most attractive is that it has a flat dynamic response (i.e., no resonances). The dynamics of the nanopositioner are defined solely by the flexure mechanism, making it possible to achieve the desired motion bandwidth through straightforward modeling of the electrostatic actuator and the structural dynamics of the flexure mechanism. The greatest challenge in using an electrostatic actuator is that the ratio of the actuation force over the in-plane actuator area is low in comparison to other actuators. As a result, large actuators are necessary to generate an adequate motion range in most cases. This limits the electrostatic actuation to applications in which the deeply scaled integration of MEMS nanopositioners arrays is not required.

9.3.2 *Electrothermal Actuators*

Electrothermal actuators are the second most popular type of actuator for MEMS nanopositioners. In these actuators, a current is passed through an electromechanical structure with an appropriate resistance (typically between 100 Ω and 1 kΩ). This results in Joule heating causing the structure to expand due to the increase in temperature. If designed correctly, the thermal expansion results in linear motion that is proportional to the voltage squared since the temperature increase is proportional to the power dissipation. By properly constraining the electromechanical structure, the actuator motion can be significantly larger than that achieved through linear expansion alone. Thermal expansion provides continuous smooth motion that can easily be controlled through the actuation voltage.

Almost all electrothermal actuators can be defined as being one of following two types: (1) Joule heating through the bulk of a single-material actuator or (2) Joule heating of stacked, thermally mismatched materials (i.e., bimorph actuation). In the first type, current flows through the bulk of the structure and the actuator uniformly expands and contracts across its cross-section. The two most common geometries for this type are the chevron actuator and the U-shape actuator, as shown in Fig. 9.10. The chevron actuator [65] has a symmetric geometry with angled beams connected to a center shuttle that transmits the force. When current flows through the beams, they heat up and their length increases, causing the center shuttle to move. The resulting output motion is related to the drive voltage, the geometry of the beams,

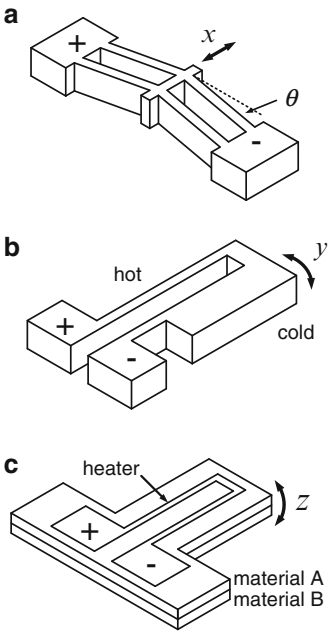

Fig. 9.10 Common electrothermal actuator designs. (**a**) chevron actuator, (**b**) U-shape actuator, and (**c**) thermal bimorph actuator

and the beam angle. A smaller beam angle provides larger motion for the same drive voltage but also reduces the actuator stiffness, thereby reducing the force that can be transmitted. Numerous MEMS nanopositioners have relied on this actuator [65–72] due to its simplicity of design and because is generates highly linear motion.

The U-shape actuator [73] is composed of a narrow beam (hot arm) and a wide beam (cold arm) that are connected in a continuous loop. When a current flows through the loop, the hot arm heats up and expands, while the cold arm experiences a much smaller increase in temperature due to its lower resistance. This mismatch in expansion causes motion at the tip of the actuator along an arc. Nanopositioning typically requires linear motion so the arc motion of the U-shape actuator is unacceptable in most cases. This has limited it use in comparison to the chevron actuator. Linear motion can be achieved though by coupling two actuators together as shown in [47] (see Fig. 9.6). The geometry shown in Fig. 9.10b and in [47, 73] is for in-plane motion. However, the principle of using a hot and cold arm has been demonstrated for out-of-plane motion as well [74].

Bimorph actuators that use Joule heating are composed of two or more materials that have different coefficients of thermal expansion and a heater, which is a conductive structure that is driven electrically (see Figs. 9.10c and 9.11). When a current is applied to the heater, the actuator heats up and moves due to internal stress caused by the mismatch in thermal expansion and the thermal gradient. This approach is most commonly used with cantilevers [16–18, 75, 76] because large motion can be generated at the cantilever tip due to small strain at the base from thermal expansion. Furthermore, it is relatively easy to stack the materials necessary to achieve a large mismatch in their expansion. As with the U-shape actuator,

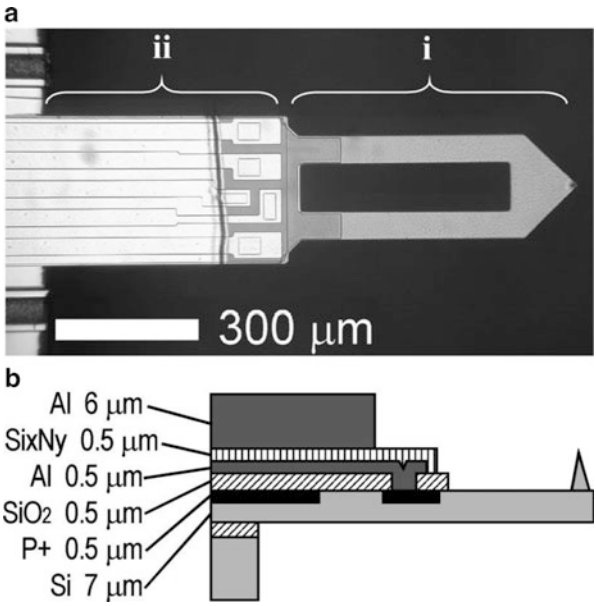

Fig. 9.11 Thermal bimorph cantilever. (**a**) Section *ii* is the thermal bimorph actuator and section *i* contains a piezoresistive sensor, (**b**) schematic of cantilever cross-section (T. Akiyama et al. © AIP [75])

bimorph cantilevers generate motion along an arc making them less attractive for nanopositioning. However, the thermal bimorph concept has been implemented to generate in-plane linear motion by using a CMOS (complementary metal-oxide semiconductor) fabrication process to create actuators composed of dielectric structures and metal heaters [23, 24, 77]. These in-plane actuators use beam bending resulting from bimorph actuation but the heaters are strategically placed within the beams and multiple bimorph beams are coupled together. This design cancels out the rotational motion typically found in bimorph actuators, thereby providing linear output motion. As a result, this design can be used in applications similar to that of the chevron actuator.

While there is considerable variation in the motion range of thermal actuators, the maximum displacement is around 20 μm. The reduced range compared to electrostatic actuators is frequently compensated using a flexure mechanism with motion amplification [28, 42]. Similar to electrostatic actuators, the displacement of electrothermal actuators is proportional to the square of the applied voltage. However, when this input nonlinearity is canceled using an analog circuit or digital signal processor, their dynamic response is nearly linear with the exception of temperature-dependent material properties. The chevron and U-shape actuators are straightforward to fabricate since they only require a single device layer, making these devices attractive for silicon-on-insulator processes.

In addition to ease of fabrication, electrothermal actuators are robust mechanisms that can withstand a large number of heating cycles, are generally unaffected by surface contamination, and are less prone to electrical breakdown compared to electrostatic actuators. The biggest disadvantage of electrothermal actuators is their bandwidth, which is limited by their thermal time response. Typically, a bandwidth in the range of 100 Hz can be achieved, although this is dependent on size, heat sinking, and whether the actuator is operating in air or vacuum. The bandwidth can be extended to some degree through open-loop control [75, 78]. Even with open-loop control, the bandwidth is limited by the maximum drive voltage that can be sustained without damage and the rate at which the actuator can lose heat. This drawback of electrothermal actuation must be strongly considered for a given application.

9.3.3 Piezoelectric Actuators

Multi-layer piezoelectric actuators, such as those shown in Fig. 9.2, are by far the most commonly used actuators in macroscale nanopositioners. Interestingly, piezoelectric actuators have found very limited use in MEMS nanopositioners. This is largely due to the small piezoelectric coefficients that can be achieved (in this case, the d_{33} coefficient), thereby requiring stacked actuators with thick layers. For example, typical multi-layer piezoelectric actuators made with lead zirconate

titanate (PZT) can achieve approximately 1 μm of displacement at 120 V for a 1 mm thick material layer. Clearly, this approach does not scale well since a 1 μm thick layer would result in only 1 nm of displacement. As a result, linear actuators in which the motion has a one-to-one correspondence to the expansion of a piezoelectric material are generally not found in MEMS with the exception of resonators, which can operate with exceptionally small motion.

One approach for achieving adequate motion range with a MEMS piezoelectric actuator is to use a bimorph cantilever design [9, 14, 15]. Expansion of the piezoelectric material causes the cantilever to bend, resulting in vertical motion of the cantilever tip. Displacements of tens of micrometers can be achieved with this approach. However, linear motion cannot be generated with this configuration, limiting its application. An intriguing approach to solving this problem uses multiple bimorph actuators to generate in-plane linear motion through out-of-plane bending, resulting in a range of a few micrometers [79]. In addition to the challenge of generating linear motion, the deposition of high-quality thin-film piezoelectric materials with properties comparable to those found in macroscale materials remains an open area of research. As a result, piezoelectric actuators are not currently practical for MEMS nanopositioners but this may change in the near future.

9.4 Sensing

The most commonly used sensors in macroscale nanopositioners are capacitive sensors and strain gauge sensors, including both metal and piezoresistive types. Laser interferometry is also used when exceptional accuracy and stability are required and cost and size are not a concern. These displacement sensors must meet a set of stringent performance requirements similar to those described for actuators in the previous section: resolution of 1 nm or below, range from 1 to 100 μm, and bandwidth of a few kilohertz. In addition, linearity and thermal stability are critical since they directly affect the motion accuracy. However, it is more difficult to define these metrics and their values are largely unreported for MEMS in the literature.

Among the MEMS sensors for linear displacement measurement, either capacitive, thermal, or piezoresistive sensors have been used in almost all MEMS nanopositioners to date, as described below. The most intriguing option that has yet to receive adequate attention is optical sensing, including interferometric [80] and diffractive optics [81] sensors. With the continued integration of photonics into MEMS, optical sensors in MEMS nanopositioners are expected over the next decade.

9.4.1 Capacitive Sensors

Capacitive sensing has been integral to a number of MEMS sensor technologies including accelerometers, gyroscopes, pressure sensors, and force sensors, and their mechanical and electronic design is well developed. This is because they can achieve exceptional displacement resolution and are easy to fabricate in standard MEMS processes. As a result, capacitive sensors are the most common displacement sensors used in MEMS nanopositioners. Capacitive sensors convert a displacement into a change in capacitance, which is measured using readout electronics. The variable capacitor designs that are typically used are the same as the electrostatic actuators shown in Fig. 9.7: the comb sensor [29, 66, 82–84], parallel-plate sensor [58], and parallel-plate sensor with comb structure [63, 64]. Similar to electrostatic actuators, the comb sensor has a linear relationship between capacitance and displacement, whereas parallel-plate designs are nonlinear. Since sensor linearity is critical in nanopositioning, the comb sensor is highly preferred. Sub-nanometer resolution has been achieved using both single-ended comb sensors, with [29, 66] and without [83] motion amplification, and with differential comb sensors [84]. Comb sensors have many of the same advantages as comb actuators, including large range, flat dynamic response, high bandwidth, and ease of fabrication.

The readout electronics that measure the change in capacitance when the nanopositioner moves are just as important as the structure of the sensor. The most sensitive readout electronics for capacitive sensors are AC bridge and switched capacitor circuits [85]. These circuits can achieve a noise floor better than 0.1 aF/rt-Hz, making it possible to reach sub-nanometer resolution, and a dynamic range above 10^5, which are ideal characteristics for nanopositioning. Furthermore, these circuits are compatible with CMOS electronics [85, 86], making it possible to integrate the MEMS and electronics on a single chip or co-integrate in a single package.

As with electrostatic actuators, the main disadvantage of comb sensors is the area required to attain a sufficiently sensitive device. An important recent innovation for capacitive sensing in nanopositioners is the use of the same comb structure for both actuation and sensing [87, 88]. This reduces the area required for actuation and sensing by half, thereby increasing its bandwidth by reducing the mass of the nanopositioner. In one configuration, the actuation signal and the AC signal used to measure the comb capacitance are separated in the frequency domain and filtering is used to lock in on the sensor signal [87]. The frequency of the AC signal is selected to be well above the mechanical resonances of the structure so that it does not impart a measurable motion. Alternatively, the comb has been used as a tunable capacitor within a resonant LC circuit [88]. The resonant frequency of the circuit is modulated by the motion of the nanopositioner, which can be calibrated to attain a sensitivity in Hz/nm. The change in frequency of the resonator can be measured using a phased locked loop, providing a high bandwidth sensor output. Actuation and sensing on the same comb has yet to be compared to the performance of independent actuation and sensing channels and warrants further investigation.

9.4.2 Thermal Sensors

Over the last decade, thermal sensors have emerged as a viable alternative to capacitive sensors for displacement measurement in MEMS [71, 72, 83, 89–92]. In its simplest form, a thermal sensor uses heat conduction between an electrothermal heater and a moving heat sink, typically the motion stage, as a measure of position. The heater is most commonly made of doped silicon and is shaped to evenly distribute the heat over the area of the heater that interacts with the motion stage. The heater and the motion stage interact through a small gap (<5 μm) that conducts heat away from the heater. As the overlapping area between the motion stage and heater changes due to displacement, the temperature of the heater changes, resulting in a change in the resistance of the heater. The change in resistance is measured with readout electronics and the output voltage is calibrated using an accurate measurement of the motion of the nanopositioner. The sensor and motion stage can be stacked vertically [72, 89, 91] or they can interact in the plane of motion [71, 83, 90]. In most cases, the thermal sensor and actuator moving the motion stage are separated to avoid coupling of their dynamics. However, it is possible to intentionally couple an electrothermal actuator to a thermal sensor, which significantly reduces the area consumed by the mechanism [91].

Thermal sensors are typically measured in pairs in which the overlapping area increases for one heater and decreases for the other for a given motion of the stage. Assuming a constant voltage across the heaters, the current flowing through one heater increases and the other decreases. By measuring the difference between the two signals, sensor drift due to environmental temperature fluctuations and sensor aging can be canceled out. This differential configuration of thermal sensors for measuring the motion of a moving stage is shown in Fig. 9.12. Trans-impedance amplifiers are used to convert the sensor currents to voltage, which are then subtracted from each other to attain the drift-free sensor output. Interestingly, when directly compared to capacitive sensing, thermal sensors yielded a lower noise floor above 4 Hz in one implementation [83], demonstrating the applicability of this approach to nanopositioning. Thermal sensors, similar to the piezoresistive sensors discussed in the next subsection, have high $1/f$ noise compared to capacitive sensors due to fluctuations in the conductivity of the heaters. This issue has been addressed through AC modulation of the heater voltage and measuring the output voltage with a lock-in amplifier at the modulation frequency, which has been shown to improve the noise floor at low frequency by a factor of 2 [92].

Among the many promising features of thermal sensors, they have been shown to be capable of a resolution of 0.5 nm, a motion range of tens of micrometers, and 10 kHz bandwidth [89]. Additionally, the majority of the sensors to date are no bigger than 400 $\mu m \times 200$ μm, which is considerably smaller than capacitive sensors. The fabrication of most existing thermal sensor designs is straightforward, particularly the in-plane design shown in Fig. 9.12 since it uses a standard silicon-on-insulator process. Sensor linearity is design dependent, with some demonstrating high linearity [89] and others with strong nonlinearity [71]. The largest drawback of

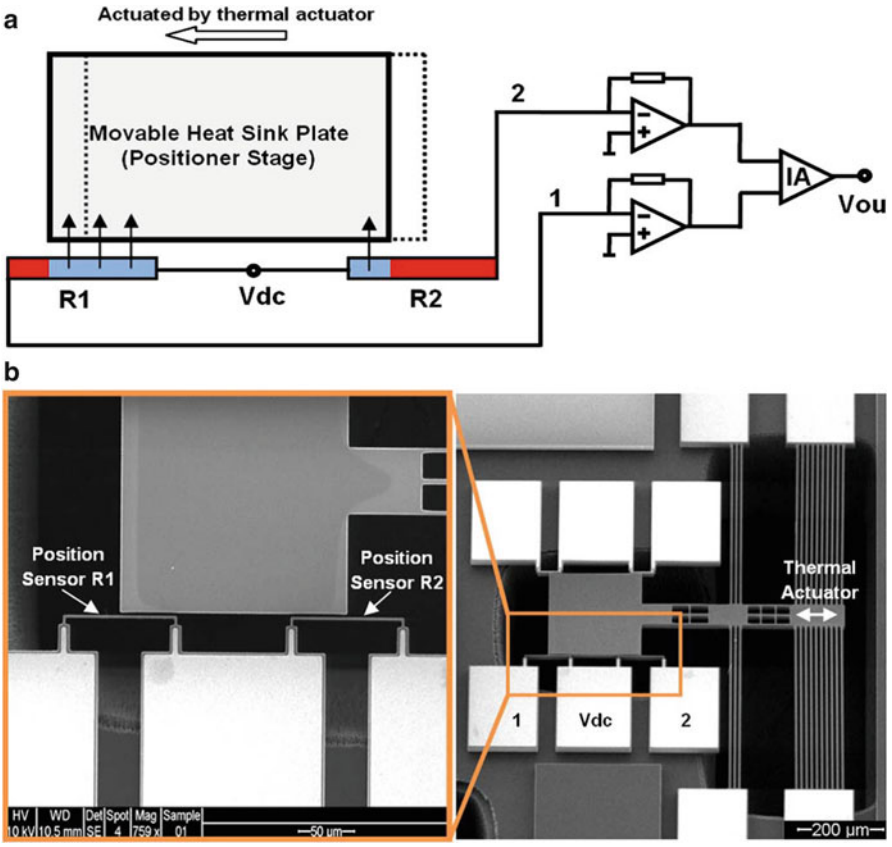

Fig. 9.12 Thermal displacement sensor with differential readout electronics. (**a**) Schematic of approach for differential readout of two thermal sensors, (**b**) scanning electron micrographs of the thermal sensors, motion stage, and the electrothermal actuator that moves the stage (Zhu et al. © IEEE [90])

thermal sensors is that they act as heat sources that can cause significant asymmetric thermal expansion in the mechanism. MEMS nanopositioners require excellent motion accuracy and stability and thermal expansion could degrade performance in these areas. This issue requires further study to determine if it will impact MEMS nanopositioner applications.

9.4.3 Piezoresistive Sensors

Piezoresistive sensing was one of the first sensing mechanisms to be used in MEMS and has been integral to many of the most common sensor products including

pressure sensors, accelerometers, gyroscopes, and microphones [93]. Piezoresistors are similar to metal strain gauges in that their resistance changes due stress. However, metal strain gauges change resistance only due to geometric changes caused by the stress. Piezoresistors, which are fabricated from semiconducting materials, most commonly silicon, also change resistance due to a stress-induced change in the bandgap of the material, which is typically a much larger effect than the change due to geometric effects. Piezoresistive sensors are frequently used in low-precision macroscale nanopositioners because they are compact, allowing them to be directly bonded to piezoelectric stack actuators. Unfortunately, their resolution is typically one to two orders of magnitude worse than capacitive sensors. The first MEMS nanopositioners to use piezoresistive sensors were cantilever arrays designed for SPM [15–18]. One example is shown in Fig. 9.4, in which four piezoresistors are located at the base of each AFM cantilever within the array. The piezoresistors are embedded in the cantilever through selective doping of silicon. This approach measures the induced strain due to the out-of-plane motion of the cantilever tip rather than measuring the tip motion directly.

Measurement of in-plane motion using piezoresistive sensors has been achieved by using suspended silicon structures that extend or compress when the nanopositioner moves. For example, long slender beams were used as piezoresistors to measure the displacement of a motion stage over a 12 μm range [94]. The piezoresistors were fabricated in the same silicon layer as the nanopositioner, as shown in Fig. 9.13, greatly simplifying fabrication since actuation and sensing are formed in the same etch step and selective doping is not required. Similar to the simultaneous actuation and sensing approach used with electrostatic comb actuators [87, 88], piezoresistive sensing can be combined with electrothermal actuation [70, 95]. The beams in a chevron electrothermal actuator experience a change in resistance during actuation due to stress and a change in resistivity due to the change in temperature. As a result, the change in resistance can be measured during actuation to attain the actuator displacement. However, due to coupling between actuation and sensing, the response is nonlinear and it is not straightforward to separate these coupling effects.

Another approach for integrating piezoresistors into flexural structures uses a CMOS–MEMS fabrication process that is also compatible with making independent electrothermal actuators [23, 24], as described in the previous section. In this case, the piezoresistors are composed of polysilicon and are embedded in a silicon dioxide structural layer. Both in-plane and out-of-plane motion can be measured by strategically placing the piezoresistors to measure the strain related to the desired degree of freedom.

There are only a handful of cases where piezoresistive sensing has been applied successfully to MEMS nanopositioners so it is difficult to quantify the expected resolution and range. Hafizovic et al. [18] demonstrated a 1 nm resolution over a 1 μm range, while Bazaei et al. [94] achieved 5 nm resolution over a range of 12 μm. While the resolution is promising, the dynamic range reported to date is quite low, with the best result among the included references being 8000. The resolution is generally limited by the high level of $1/f$ noise and Johnson noise that is universal

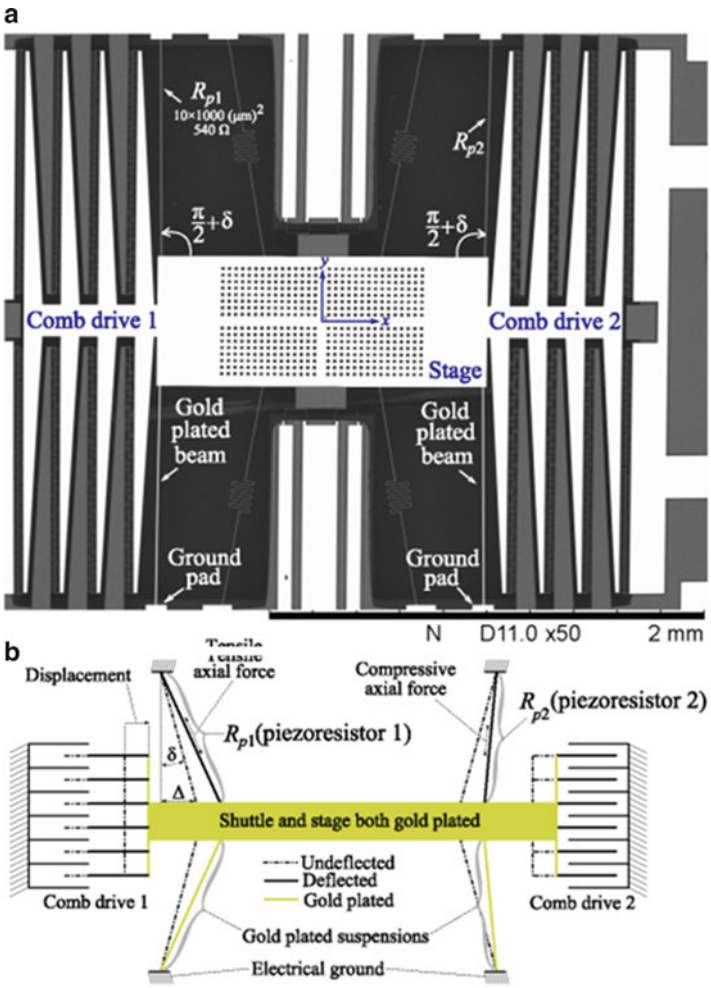

Fig. 9.13 MEMS nanopositioner with piezoresistive sensors. (**a**) Scanning electron micrograph showing thin silicon piezoresistors (R_{p1} and R_{p2}) connected to the motion stage, (**b**) Schematic describing the strain in each piezoresistor due to stage motion (Bazaei et al. © IEEE [94])

to all resistors. The use of AC readout electronics can eliminate the contribution from the $1/f$ noise, but the Johnson noise is still a major contributor to the noise floor.

The biggest advantages of piezoresistive sensors are their small size, thereby minimizing the overall area consumed by a mechanism, and their high bandwidth, which is typically limited by the structural dynamics of the flexure mechanism and the readout electronics. Attaining piezoresistors with a high gauge factor (i.e., high sensitivity) typically requires selective ion implantation or diffusion doping, complicating the fabrication process. However, adequate displacement resolution

has been achieved without selective doping [94], so a high gauge factor may not be required in some applications. Thermal drift is another well-known problem with piezoresistors that could be a perceived issue for MEMS nanopositioners. However, this problem is easily mitigated by using a full Wheatstone bridge to readout the resistance change and by including reference piezoresistors in the design that do not experience stress. In general, piezoresistive sensors are an intriguing approach for displacement measurement in MEMS nanopositioners that requires more research to determine whether sub-nanometer resolution can be achieved over tens of micrometers of motion.

9.5 Performance Assessment

A number of different MEMS nanopositioners have been described in the previous sections. An open question is whether these mechanisms can perform as well as macroscale nanopositioners. Although this is a difficult question to answer since many of the performance characteristics of interest are rarely reported, this section provides an assessment of the performance of existing MEMS nanopositioners and compares the results with the typical performance achieved at the macroscale. The focus of this comparison is on the aggregate rather than highlighting the top performing mechanisms and does not examine the effect of actuator and sensor selection on performance. The following subsection discusses the methodology for the assessment and is followed by the presentation and discussion of the results.

9.5.1 Methodology

Four performance metrics have been selected for this assessment: range, resolution, bandwidth, and in-plane area. Data was cataloged from the relevant references previously cited in this chapter and [96–103], with 59 references providing usable data points. A minimum of the in-plane area and one other metric were required for a reference to be included in this analysis. The range is defined as either a stated value or the maximum displacement presented in the reference. Resolution is defined as either the stated RMS resolution or is calculated from the displacement noise floor in $m/Hz^{1/2}$ using the bandwidth. Due to $1/f$ noise and other noise sources, there can be a considerable difference between the RMS noise and that calculated using the noise floor and bandwidth. However, this is unavoidable for this assessment since resolution is so rarely stated explicitly. The bandwidth is taken as the lowest value among the stated bandwidth, the half-power point of the amplitude frequency response, and the first resonant frequency. Finally, the in-plane area is typically extracted from provided images and is defined as the width multiplied by the length. For mechanisms with multiple degrees of freedom, the width and length are divided by the degrees of freedom to provide a fair comparison with single axis devices.

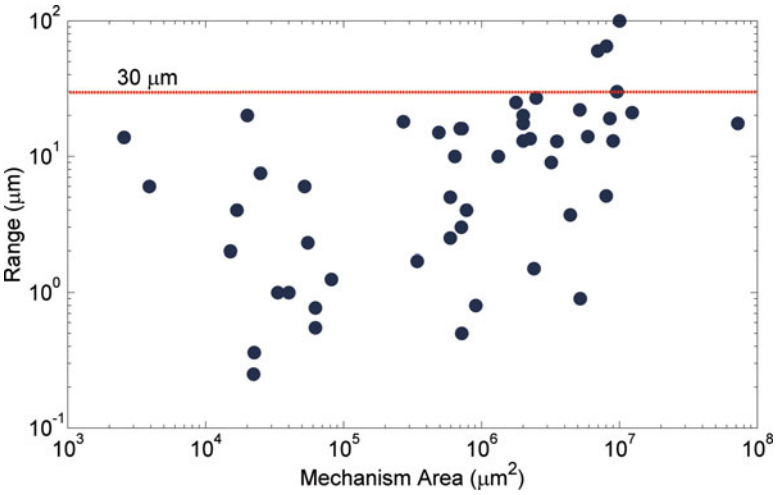

Fig. 9.14 Range as a function of in-plane mechanism area for MEMS nanopositioners

9.5.2 Results

Among the four metrics of interest, range is the most widely reported. Comparing motion range versus in-plane area, as shown in Fig. 9.14, there is a wide distribution in both of these metrics. Most MEMS nanopositioners have a range below 30 μm with some exceptions going to 100 μm and beyond (some outliers were not included in the figures). This is shorter than the average range for macroscale nanopositioners but is expected for MEMS and 30 μm is sufficient for many of the applications of interest. One clear trend is that larger area is required for the longest-range mechanisms, which is obvious since more force and larger flexure mechanisms are required for large range. More interesting is that below 10 μm the same range is achieved by mechanisms ranging in area from 10^4 to 10^7 μm^2. This is due in part to the trade-offs in actuator selection and the common use of flexure mechanisms that are not optimized for the expected range, resulting in excessively large dimensions.

Resolution is the single most important performance metric since it determines whether a motion stage can truly achieve nanoscale motion precision. Unfortunately, achieving a clear assessment of resolution is challenging since multiple definitions are used including the RMS value of the displacement noise and the displacement noise floor. Furthermore, it is commonly not addressed in publications; less than half of the references providing range data also include resolution. Finally, independent confirmations of resolution, as done with a laser interferometer at the macroscale, are rare. Even with these challenges, there are some useful insights attained by looking at resolution as a function of in-plane area, as shown in Fig. 9.15. Similar to the range data, there is a wide distribution for resolution, spanning more than two orders of magnitude. Most of the available data is for larger mechanisms (≈1 mm^2 or larger) but there is no obvious trend indicating a relationship between scale and

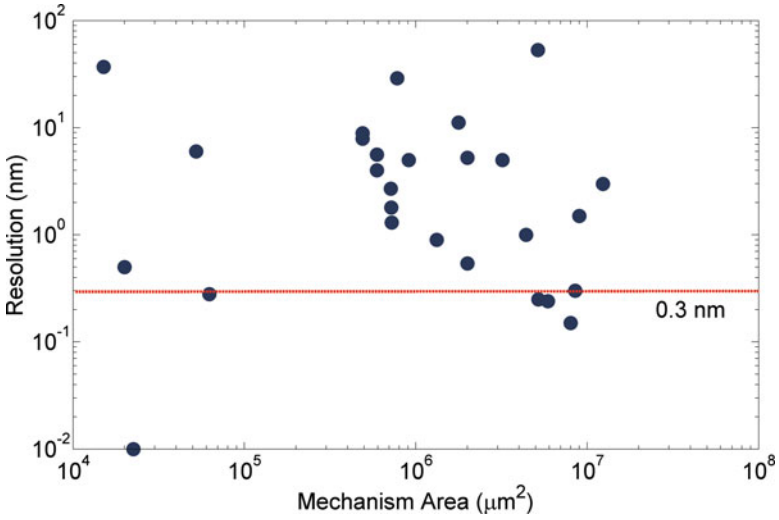

Fig. 9.15 Resolution as a function of in-plane mechanism area for MEMS nanopositioners

resolution. In terms of magnitude, there are a handful of papers reporting sub-nanometer resolution but the majority of mechanisms are above 2 nm, making it difficult to define them as nanopositioners.

As previously discussed, the dynamic range (DR) (i.e., range/resolution) for macroscale nanopositioners is typically greater than 10^5. Assuming that the range is below 30 μm as described in the previous paragraph and a DR = 10^5, the resolution should be less than 0.3 nm as indicated by the dashed line in Fig. 9.15. It is clear that only a few reported designs can perform at this level. Taking another look at this issue, range versus resolution is plotted in Fig. 9.16 along with contour lines for dynamic range. The majority of reported designs perform below DR = 10^4 and no MEMS nanopositioner considered in this analysis has achieved a DR $\geq 10^5$. This is the single greatest limitation in the state of the art. The resolution needs to be improved to meet that achieved at the macroscale while also increasing the dynamic range beyond 10^5 (i.e., improve resolution while not decreasing range).

As expected, bandwidth is the metric in which MEMS nanopositioners show exceptional performance, as shown in Fig. 9.17. Most reported mechanisms have bandwidth greater than 100 Hz and more than half have demonstrated bandwidth greater than 1 kHz. This bandwidth range is sufficient for many applications and can clearly be further optimized considering some examples above 10 kHz have been demonstrated. The data in Fig. 9.17 shows that, as expected, bandwidth is linked to in-plane area with the greatest bandwidth occurring on the low end of the spectrum (200 kHz at 6×10^4 μm^2) and the smallest bandwidth at the high end (20 Hz at 7×10^6 μm^2). Based on Figs. 9.14, 9.15, and 9.17, the majority of MEMS nanopositioners to date have an area greater than 2.5×10^5 μm^2 (i.e., equivalent to a 500 μm square). Reduction in this area would improve bandwidth and facilitate large-scale integration of arrays for scanning probe applications.

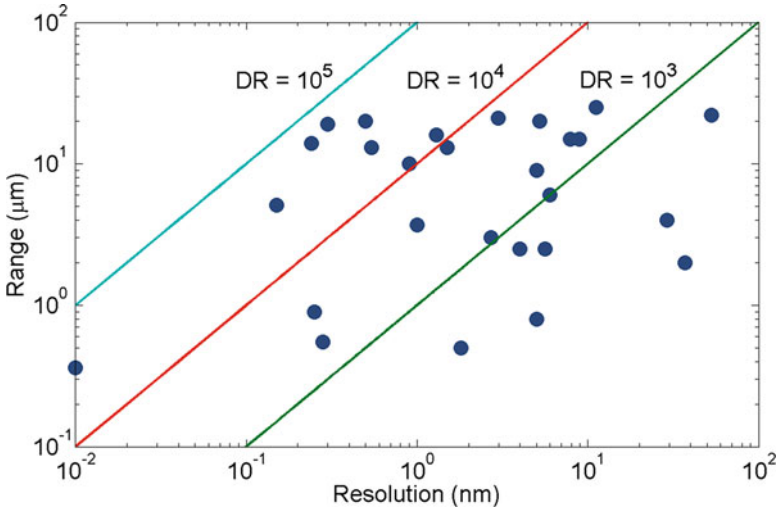

Fig. 9.16 Range as a function of resolution for MEMS nanopositioners. *DR* dynamic range

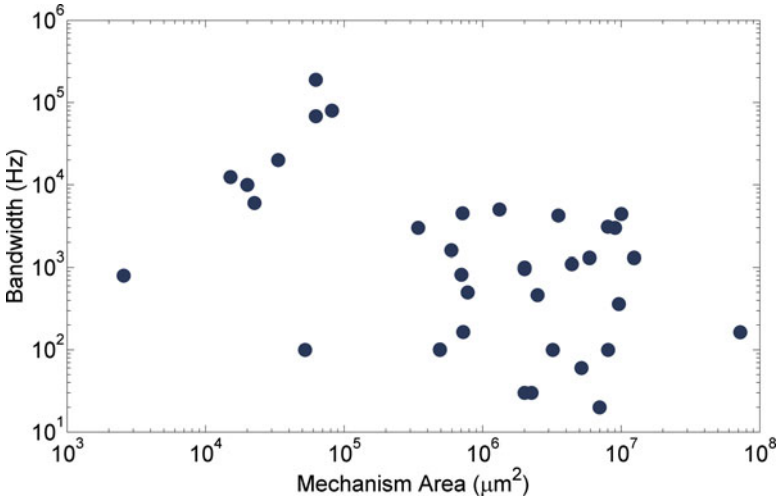

Fig. 9.17 Bandwidth as a function of in-plane mechanism area for MEMS nanopositioners

While the presented data and analysis is clearly not complete it does provide some important insights into the state of the art. The range and bandwidth of existing mechanisms are adequate for known applications and in some cases the bandwidth is exceptional compared to non-MEMS approaches. Unfortunately, the resolution and dynamic range found in this analysis are both worse than that found in macroscale nanopositioners by an order of magnitude or more in most cases. This provides a clear direction for future research with a goal of achieving resolution <0.1 nm RMS and DR > 10^5.

9.6 Conclusion

MEMS nanopositioners have emerged over the last two decades as a highly capable class of mechanisms that merges precision engineering design principles with MEMS sensors and actuators. They are already being used successfully in SPM and probe-based data storage, with products expected within the next few years, and hold promise in many other applications (e.g., nanomanufacturing, nanomaterial testing, biomedical, photonics). This chapter has provided an overview of the critical components within these mechanisms, provided discussion on the advantages and disadvantages of the most common actuators and sensors, and presented a meta-analysis of their performance to date.

Among the possible actuator technologies of interest, electrostatic, electrothermal, and piezoelectric actuators were identified as the most compatible and widely used with MEMS nanopositioners. Piezoelectric actuators still require substantial research to reach the current performance levels achieved by the other two approaches, particularly with respect to piezoelectric material deposition and actuator design. Selection between electrostatic and electrothermal actuation can be determined almost solely on bandwidth requirements. Bandwidth above a few hundred hertz requires electrostatic actuation in most cases because the thermal response of electrothermal actuators is typically too slow. Otherwise, electrothermal actuators are preferred over electrostatic actuators when their low bandwidth can be tolerated because they require lower actuation voltage, consume less area, and are more reliable.

The most commonly used sensing approaches for MEMS nanopositioners are capacitive, thermal, and piezoresistive sensors. While capacitive sensing has been most commonly used in precision MEMS applications, thermal and piezoresistive sensing have been shown to achieve resolution and range performance that is approaching that of capacitive sensing in some situations. Furthermore, unlike the actuators discussed above, all three approaches provide adequate bandwidth for almost all nanopositioning applications. As a result, sensor selection must be based on available in-plane area (capacitive sensing takes the most area), the intended fabrication process (piezoresistive sensing is maximized by local ion implantation or diffusion doping), and the operating environment (thermal sensors are less sensitive in vacuum), among other factors. A detailed study of the three sensor types that compares their performance limits under equivalent constraints and operating conditions would be highly beneficial to future nanopositioner designs.

The presented performance assessment of existing MEMS nanopositioners revealed two deficiencies in the state of the art. First, the achievable resolution in the majority of devices reported in the study is worse by an order of magnitude or more in comparison to macroscale nanopositioners. A resolution of 0.1 nm RMS is commonly achieved in macroscale nanopositioners but most MEMS nanopositioners are above 1 nm. Second, the dynamic range among the studied mechanisms was found to be an order of magnitude worse than their macroscale counterparts ($>10^5$) in most cases. Somewhat less critical, it was found that that the majority of MEMS

nanopositioners have an in-plane area greater than 2.5×10^5 μm^2, or a 500 μm square. This size limitation should be improved because it currently restricts the capabilities of nanopositioner arrays due to poor fill factor. The other performance metrics of interest, range, and bandwidth have been shown to be adequate in many of the existing mechanisms.

Looking to the future, research should be focused on improving resolution and dynamic range since these metrics are the best indicators of usability in nanopositioning applications and the state of the art is inadequate. If 0.1 nm RMS resolution and a dynamic range above 10^5 can be achieved, MEMS nanopositioners will be capable of replacing macroscale nanopositioners in scanning probe applications. Another area that warrants more attention is the integration of scanner arrays with independent *XYZ* motion. Previous work on parallel operation has focused on cantilever arrays with a single degree of freedom in each cantilever. Recent developments in on-chip AFMs [24] have opened the door for independent scanning probe arrays that will be significantly faster and more fault tolerant than existing cantilever arrays. Embedded integration of the mechanisms and electronics will be critical to the success of such systems. Other important areas of research include analysis of positioning stability, cross talk between axes, and the limitations of actuation and readout electronics. With sustained efforts in these research areas, it is expected that MEMS nanopositioners will outperform macroscale nanopositioners within the following decade.

References

1. J.W. Ryu, D.-G. Gweon, K.S. Moon, Optimal design of a flexure hinge based XYφ wafer stage. Precis. Eng. **21**, 18–28 (1997)
2. P. Gao, S.-M. Swei, Z. Yuan, A new piezodriven precision micropositioning stage utilizing flexure hinges. Nanotechnology **10**, 394–398 (1999)
3. A. Elmustafa, M.G. Lagally, Flexural-hinge guided motion nanopositioner stage for precision machining: finite element simulations. Precis. Eng. **25**, 77–81 (2001)
4. http://www.physikinstrumente.com
5. http://www.npoint.com
6. http://www.aerotech.com
7. S. Salapaka, A. Sebastian, J.P. Cleveland, M.V. Salapaka, High bandwidth nano-positioner: a robust control approach. Rev. Sci. Instrum. **73**, 3232–3241 (2002)
8. C.-W. Lee, S.-W. Kim, An ultraprecision stage for alignment of wafers in advanced microlithography. Precis. Eng. **21**, 113–122 (1997)
9. S. Akamine, T.R. Albrecht, M.J. Zdeblick, C.F. Quate, Microfabricated scanning tunneling microscope. IEEE Electron Device Lett. **10**, 490–492 (1989)
10. E. Meyer, H.J. Hug, R. Bennwitz, *Scanning Probe Microscopy: The Lab on a Tip* (Springer, New York, 2004)
11. J.J. Yao, S.C. Arney, N.C. MacDonald, Fabrication of high frequency two-dimensional nanoactuators for scanned probe devices. J. Microelectromech. Syst. **1**, 14–22 (1992)
12. Y. Xu, N.C. MacDonald, S.A. Miller, Integrated micro-scanning tunneling microscope. Appl. Phys. Lett. **67**, 2305–2307 (1995)

13. S.A. Miller, K.L. Turner, N.C. MacDonald, Microelectromechanical scanning probe instruments for array architectures. Rev. Sci. Instrum. **68**, 4155–4162 (1997)
14. S.C. Minne, J.D. Adams, G. Yaralioglu, S.R. Manalis, A. Atalar, C.F. Quate, Centimeter scale atomic force microscope imaging and lithography. Appl. Phys. Lett. **73**, 1742–1744 (1998)
15. S.C. Minne, G. Yaralioglu, S.R. Manalis, J.D. Adams, J. Zesch, A. Atalar, C.F. Quate, Automated parallel high-speed atomic force microscopy. Appl. Phys. Lett. **72**, 2340–2342 (1998)
16. D. Lange, T. Akiyama, C. Hagleitner, A. Tonin, H.R. Hidber, P. Niedermann, U. Staufer, N.F. de Rooij, O. Brand, H. Baltes, Parallel scanning AFM with on-chip circuitry in CMOS technology, in *Proceedings of IEEE MEMS* (IEEE, New York, 1999), pp. 447–452
17. T. Volden, M. Zimmermann, D. Lange, O. Brand, H. Baltes, Dynamics of CMOS-based thermally actuated cantilever arrays for force microscopy. Sensors Actuators A **115**, 516–522 (2004)
18. S. Hafizovic, D. Barrettino, T. Volden, J. Sedivy, K.U. Kirstein, O. Brand, A. Hierlemann, Single chip mechatronic microsystem for surface imaging and force response studies. Proc. Natl. Acad. Sci. **101**, 17011–17015 (2004)
19. A.G. Fowler, A.N. Laskovski, A.C. Hammond, S.O.R. Moheimani, A 2-DOF electrostatically actuated MEMS nanopositioner for on-chip AFM. J. Microelectromech. Syst. **21**, 771–773 (2012)
20. A. Mohammadi, A.G. Fowler, Y.K. Yong, S.O.R. Moheimani, A feedback controlled MEMS nanopositioner for on-chip high-speed AFM. J. Microelectromech. Syst. **23**, 610–619 (2014)
21. M. Maroufi, A. Bazaei, S.O.R. Moheimani, A high-bandwidth MEMS nanopositioner for on-chip AFM: design, characterization, and control. IEEE Trans. Control Syst. Technol. **23**, 504–512 (2015)
22. M. Maroufi, A.G. Fowler, A. Bazaei, S.O.R. Moheimani, High-stroke silicon-on-insulator MEMS nanopositioner: control design for non-raster scan atomic force microscopy. Rev. Sci. Instrum. **86**, 023705 (2015)
23. N. Sarkar, G. Lee, R.R. Mansour, CMOS-MEMS dynamic FM atomic force microscope, in *Proceedings of Transducers* (IEEE, New York, 2013), pp. 916–919
24. N. Sarkar, D. Strathearn, G. Lee, M. Olfat, R.R. Mansour, A 0.25 mm^3 atomic force microscope on-a-chip, in *Proceedings of IEEE MEMS* (IEEE, New York, 2015), pp. 732–735
25. E. Eleftheriou et al., Millipede – a MEMS-based scanning-probe data-storage system. IEEE Trans. Magn. **39**, 938–945 (2003)
26. Y. Ahn, T. Ono, M. Esahi, Si multiprobes integrated with lateral actuators for independent scanning probe applications. J. Micromech. Microeng. **15**, 1224–1229 (2005)
27. N. Sarkar, C. Baur, E. Stach, Z. Jandric, R. Stallcup, M. Ellis et al., Modular MEMS experimental platform for transmission electron microscopy, in *Proceedings of IEEE MEMS* (IEEE, New York, 2006), pp. 146–149
28. J.J. Gorman, Y.-S. Kim, A.E. Vladar, N.G. Dagalakis, Design of an on-chip microscale nanoassembly system. Int. J. Nanomanuf. **1**, 710–721 (2007)
29. X. Liu, J. Tong, Y. Sun, A millimeter-sized nanomanipulator with sub-nanometer positioning resolution and large force output. Smart Mater. Struct. **16**, 1742–1750 (2007)
30. S. Lu, D.A. Dikin, S. Zhang, F.T. Fisher, J. Lee, R.S. Ruoff, Realization of nanoscale resolution with a micromachined thermally actuated testing stage. Rev. Sci. Instrum. **75**, 2154–2162 (2004)
31. Y. Zhu, H.D. Espinosa, An electromechanical material testing system for in situ electron microscopy and applications. Proc. Natl. Acad. Sci. **102**, 14503–14508 (2005)
32. B. Pant, B.L. Allen, T. Zhu, K. Gall, O.N. Pierron, A versatile microelectromechanical system for nanomechanical testing. Appl. Phys. Lett. **98**, 053506 (2011)
33. S.T. Smith, D.G. Chetwynd, *Foundations of Ultra-Precision Mechanism Design* (CRC Press, Boca Raton, 1992)
34. S.T. Smith, *Flexures: Elements of Elastic Mechanisms* (Taylor & Francis, London, 2000)

35. R. Legtenberg, A.W. Groeneveld, M. Elwenspoek, Comb-drive actuators for large displacements. J. Micromech. Microeng. **6**, 320–329 (1996)
36. V.P. Jaecklin, C. Linder, N.F. de Rooij, J.M. Moret, R. Bischof, F. Rudolf, Novel polysilicon comb actuators for XY-stages, in *Proceedings of IEEE MEMS* (IEEE, New York, 1992), pp. 147–149
37. D. Kobayashi, T. Hirano, T. Furuhata, H. Fujita, An integrated lateral tunneling unit, in *Proceedings of IEEE MEMS* (IEEE, New York, 1992), pp. 214–219
38. M.I. Lutwyche, Y. Wada, Manufacture of micromechanical scanning tunnelling microscopes for observation of the tip apex in a transmission electron microscope. Sensors Actuators A **48**, 127–136 (1995)
39. C.S.B. Lee, S. Han, N.C. MacDonald, Single crystal silicon (SCS) XY-stage fabricated by DRIE and IR alignment, in *Proceedings of IEEE MEMS* (IEEE, New York, 2000), pp. 28–33
40. C.-H. Kim, Y.-K. Kim, Micro XY-stage using silicon on a glass substrate. J. Micromech. Microeng. **12**, 103–107 (2002)
41. J. Dong, D. Mukhopadhyay, P.M. Ferreira, Design, fabrication and testing of a silicon-on-insulator (SOI) MEMS parallel kinematics XY stage. J. Micromech. Microeng. **17**, 1154–1161 (2007)
42. Y.-S. Kim, J.-M. Yoo, S.H. Yang, Y.-M. Choi, N.G. Dagalakis, S.K. Gupta, Design, fabrication and testing of a serial kinematic MEMS XY stage for multifinger manipulation. J. Micromech. Microeng. **22**, 085029 (2012)
43. X. Liu, K. Kim, Y. Sun, A MEMS stage for 3-axis nanopositioning. J. Micromech. Microeng. **17**, 1796–1802 (2007)
44. J. Dong, P.M. Ferreira, Electrostatically actuated cantilever with SOI-MEMS parallel kinematic XY stage. J. Microelectromech. Syst. **18**, 641–651 (2009)
45. Y.S. Kim, N.G. Dagalakis, S.K. Gupta, Design of MEMS based three-axis motion stage by incorporating a nested structure. J. Micromech. Microeng. **24**, 075009 (2014)
46. D. Mukhopadhyay, J. Dong, E. Pengwang, P. Ferreira, A SOI-MEMS-based 3-DOF planar parallel-kinematics nanopositioning stage. Sens. Actuators A **147**, 340–351 (2008)
47. S.-C. Chen, M.L. Culpepper, Design of a six-axis micro-scale nanopositioner—μHexFlex. Precis. Eng. **30**, 314–324 (2006)
48. S.D. Senturia, *Microsystem Design* (Springer, New York, 2001)
49. C. Liu, *Foundations of MEMS* (Prentice Hall, Upper Saddle River, 2011)
50. D.J. Bell, T.J. Lu, N.A. Fleck, S.M. Spearing, MEMS actuators and sensors: observations on their performance and selection for purpose. J. Micromech. Microeng. **15**, S153–S164 (2005)
51. N.B. Hubbard, M.L. Culpepper, L.L. Howell, Actuators for micropositioners and nanopositioners. Appl. Mech. Rev. **59**, 324–334 (2006)
52. R.C. Batra, M. Porfiri, D. Spinello, Review of modeling electrostatically actuated microelectromechanical systems. Smart Mater. Struct. **16**, R23–R31 (2007)
53. Y.-M. Choi, J.J. Gorman, N.G. Dagalakis, S.H. Yang, Y.-S. Kim, J.-M. Yoo, A high-bandwidth electromagnetic MEMS motion stage for scanning applications. J. Micromech. Microeng. **22**, 105012 (2012)
54. J.D. Grade, H. Jerman, T.W. Kenny, Design of large deflection electrostatic actuators. J. Microelectromech. Syst. **12**, 335–343 (2003)
55. M. Olfatnia, S. Sood, J.J. Gorman, S. Awtar, Large stroke electrostatic comb-drive actuators enabled by a novel flexure mechanism. J. Microelectromech. Syst. **22**, 483–494 (2013)
56. T. Akiyama, U. Staufer, N.F. de Rooij, Atomic force microscopy using an integrated comb-shape electrostatic actuator for high-speed feedback motion. Appl. Phys. Lett. **76**, 3139–3141 (2000)
57. J.L.A. Yeh, C.-Y. Hui, N.C. Tien, Electrostatic model for an asymmetric combdrive. J. Microelectromech. Syst. **9**, 126–135 (2000)
58. M.S.C. Lu, G.K. Fedder, Position control of parallel-plate microactuators for probe-based data storage. J. Microelectromech. Syst. **13**, 759–769 (2004)
59. A.G. Onaran, M. Balantekin, W. Lee, W.L. Hughes, B.A. Buchine, R.O. Guldiken et al., A new atomic force microscope probe with force sensing integrated readout and active tip. Rev. Sci. Instrum. **77**, 023501 (2006)

60. E.C.M. Disseldorp, F.C. Tabak, A.J. Katan, M.B.S. Hesselberth, T.H. Oosterkamp, J.W.M. Frenken et al., MEMS-based high speed scanning probe microscopy. Rev. Sci. Instrum. **81**, 043702 (2010)
61. F.C. Tabak, E.C.M. Disseldorp, G.H. Wortel, A.J. Katan, M.B.S. Hesselberth, T.H. Oosterkamp et al., MEMS-based fast scanning probe microscopes. Ultramicroscopy **110**, 599–604 (2010)
62. E.S. Hung, S.D. Senturia, Extending the travel range of analog-tuned electrostatic actuators. J. Microelectromech. Syst. **8**(4), 497–505 (1999)
63. D.A. Horsley, N. Wongkomet, R. Horowitz, A.P. Pisano, Precision positioning using a microfabricated electrostatic actuator. IEEE Trans. Magn. **35**, 993–999 (1999)
64. Y. Sun, D. Piyabongkarn, A. Sezen, B.J. Nelson, R. Rajamani, A high-aspect-ratio two-axis electrostatic microactuator with extended travel range. Sens. Actuators A **102**, 49–60 (2002)
65. R. Cragun, L.L. Howell, Linear thermomechanical microactuators, in *Proceedings of ASME IMECE* (ASME, New York, 1999), pp. 181–188
66. L.L. Chu, Y.B. Gianchandani, A micromachined 2D positioner with electrothermal actuation and sub-nanometer capacitive sensing. J. Micromech. Microeng. **13**, 279–285 (2003)
67. N.B. Hubbard, L.L. Howell, Design and characterization of a dual-stage, thermally actuated nanopositioner. J. Micromech. Microeng. **15**, 1482–1493 (2005)
68. S. ergna, J.J. Gorman, N.G. Dagalakis, Design and modeling of thermally actuated MEMS nanopositioners, in *Proceedings of ASME International Mechanical Engineering Congress and Exposition* (ASME, New York, 2005), pp. 561–568
69. J.J. Gorman, Y.-S. Kim, N.G. Dagalakis, Control of MEMS nanopositioners with nano-scale resolution, in *Proceedings of ASME International Mechanical Engineering Congress and Exposition* (ASME, New York, 2006), pp. 151–159
70. R.K. Messenger, Q.T. Aten, T.W. McLain, L.L. Howell, Piezoresistive feedback control of a MEMS thermal actuator. J. Microelectromech. Syst. **18**, 1267–1278 (2009)
71. Y. Zhu, A. Bazaei, S.O.R. Moheimani, M.R. Yuce, Design, modeling, and control of a micromachined nanopositioner with integrated electrothermal actuation and sensing. J. Microelectromech. Syst. **20**, 711–719 (2011)
72. M. Rakotondrabe, A.G. Fowler, S.O.R. Moheimani, Control of a novel 2-DoF MEMS nanopositioner with electrothermal actuation and sensing. IEEE Trans. Control Syst. Technol. **22**, 1486–1497 (2014)
73. J.H. Comtois, V.M. Bright, M.W. Phipps, Thermal microactuators for surface-micromachining processes, in *Proceedings of SPIE 2642, Micromachined Devices and Components* (SPIE, Bellingham, 1995), pp. 10–21
74. D. Yan, A. Khajepour, R. Mansour, Design and modeling of a MEMS bidirectional vertical thermal actuator. J. Micromech. Microeng. **14**, 841–850 (2004)
75. T. Akiyama, U. Staufer, N.F. de Rooij, Fast driving technique for integrated thermal bimorph actuator toward high-throughput atomic-force microscopy. Rev. Sci. Instrum. **73**, 2643–2646 (2002)
76. G. Vitellaro, G. L'Episcopo, C. Trigona, B. Ando, S. Baglio, A compliant MEMS device for out-of-plane displacements with thermo-electric actuation. J. Microelectromech. Syst. **23**, 661–671 (2014)
77. P.J. Gilgunn, L. Jingwei, N. Sarkar, G.K. Fedder, CMOS-MEMS lateral electrothermal actuators. J. Microelectromech. Syst. **17**, 103–114 (2008)
78. D.O. Popa, B.H. Kang, J.T. Wen, H.E. Stephanou, G. Skidmore, A. Geisberger, Dynamic modeling and input shaping of thermal bimorph MEMS actuators, in *Proceedings of IEEE ICRA* (IEEE, New York, 2003), pp. 1470–1475
79. K.R. Oldham, J.S. Pulskamp, R.G. Polcawich, M. Dubey, Thin-Film PZT lateral actuators with extended stroke. J. Microelectromech. Syst. **17**, 890–899 (2008)
80. M.W. Pruessner, T.H. Stievater, W.S. Rabinovich, In-plane microelectromechanical resonator with integrated Fabry–Pérot cavity. Appl. Phys. Lett. **92**, 081101 (2008)
81. U. Krishnamoorthy, R.H. Olsson III, G.R. Bogart, M.S. Baker, D.W. Carr, T.P. Swiler, P.J. Clews, In-plane MEMS-based nano-g accelerometer with sub-wavelength optical resonant sensor. Sens. Actuator A **145–146**, 283–290 (2008)

82. L. Ji, Y. Zhu, S.O.R. Moheimani, M.R. Yuce, A micromachined 2DOF nanopositioner with integrated capacitive displacement sensor, in *Proceedings of IEEE Sensors* (IEEE, New York, 2010), pp. 1464–1467
83. Y. Zhu, S.O.R. Moheimani, M.R. Yuce, Simultaneous capacitive and electrothermal position sensing in a micromachined nanopositioner. IEEE Electron Device Lett. **32**, 1146–1148 (2011)
84. B. Koo, X. Zhang, J. Dong, S.M. Salapaka, P.M. Ferreira, A 2 degree-of-freedom SOI-MEMS translation stage with closed-loop positioning. J. Microelectromech. Syst. **21**, 13–22 (2012)
85. N. Yazdi, H. Kulah, K. Najafi, Precision readout circuits for capacitive microaccelerometers, in *Proceedings of IEEE Sensors* (IEEE, New York, 2004), pp. 28–31
86. J. Wu, G.K. Fedder, L.R. Carley, A low-noise low-offset capacitive sensing amplifier for a 50 μm/rt-Hz monolithic CMOS MEMS accelerometer. IEEE J. Solid-State Circuits **39**, 722–730 (2004)
87. J. Dong, P.M. Ferreira, Simultaneous actuation and displacement sensing for electrostatic drives. J. Micromech. Microeng. **18**, 035011 (2008)
88. S.I. Moore, S.O.R. Moheimani, Displacement measurement with a self-sensing MEMS electrostatic drive. J. Microelectromech. Syst. **23**, 511–513 (2014)
89. M.A. Lantz, G.K. Binnig, M. Despont, U. Drechsler, A micromechanical thermal displacement sensor with nanometre resolution. Nanotechnology **16**, 1089–1094 (2005)
90. Y. Zhu, A. Bazaei, S.O.R. Moheimani, M.R. Yuce, A micromachined nanopositioner with on-chip electrothermal actuation and sensing. IEEE Electron Device Lett. **31**, 1161–1163 (2010)
91. J. Chow, Y. Lai, Displacement sensing of a micro-electro-thermal actuator using a monolithically integrated thermal sensor. Sens. Actuators A **150**, 137–143 (2009)
92. A. Mohammadi, M.R. Yuce, S.O.R. Moheimani, A low-flicker-noise MEMS electrothermal displacement sensing technique. J. Microelectromech. Syst. **21**, 1279–1281 (2012)
93. A.A. Barlian, W.-T. Park, J.R. Mallon Jr., A.J. Rastegar, B.L. Pruitt, Review: semiconductor piezoresistance for microsystems. Proc. IEEE **97**, 513–552 (2009)
94. A. Bazaei, M. Maroufi, A. Mohammadi, S.O.R. Moheimani, Displacement sensing with silicon flexures in MEMS nanopositioners. J. Microelectromech. Syst. **23**, 502–504 (2014)
95. J. Ouyang, Y. Zhu, Z-shaped MEMS thermal actuators: piezoresistive self-sensing and preliminary results for feedback control. J. Microelectromech. Syst. **21**, 596–604 (2012)
96. Y. Ando, T. Ikehara, S. Matsumoto, Design, fabrication and testing of new comb actuators realizing three-dimensional continuous motions. Sens. Actuators A **97–98**, 579–586 (2002)
97. C.-H. Kim, H.-M. Jeong, J.-U. Jeon, Y.-K. Kim, Silicon micro XY-stage with a large area shuttle and no-etching holes for SPM-based data storage. J. Microelectromech. Syst. **12**, 470–478 (2003)
98. Y. Ando, Development of three-dimensional electrostatic stages for scanning probe microscope. Sensors Actuators A **114**, 285–291 (2004)
99. L. Gu, X. Li, H. Bao, B. Liu, Y. Wang, M. Liu et al., Single-wafer-processed nano-positioning XY-stages with trench-sidewall micromachining technology. J. Micromech. Microeng. **16**, 1349–1357 (2006)
100. X. Chen, D.-W. Lee, Integrated microactuation scanning probe microscopy system. J. Vac. Sci. Technol. B **27**, 1408–1412 (2009)
101. Y.-S. Kim, N.G. Dagalakis, S.K. Gupta, Creating large out-of-plane displacement electrothermal motion stage by incorporating beams with step features. J. Micromech. Microeng. **23**, 055008 (2013)
102. A.G. Fowler, A. Bazaei, S.O.R. Moheimani, Design and analysis of nonuniformly shaped heaters for improved MEMS-based electrothermal displacement sensing. J. Microelectromech. Syst. **22**, 687–694 (2013)
103. X. Zhang, B. Koo, S.M. Salapaka, J. Dong, P.M. Ferreira, Robust control of a MEMS probing device. IEEE/ASME Trans. Mechatron. **19**, 100–108 (2014)